

**Self-Driven Membrane Filtration by Core-shell Polymer Composites**

| | |
|-------------------------------|---|
| Journal: | <i>Journal of Materials Chemistry A</i> |
| Manuscript ID | TA-ART-04-2020-003617.R2 |
| Article Type: | Paper |
| Date Submitted by the Author: | 23-May-2020 |
| Complete List of Authors: | Dou, Zeou; Georgia Institute of Technology, Wang, Ting; Georgia Institute of Technology, Civil and Environmental Engineering Chen, Wensj; Georgia Institute of Technology, Civil and Environmental Engineering Lin, Beichen; Georgia Institute of Technology, Civil and Environmental Engineering Dong, Hai; Georgia Institute of Technology Sun, Wei; Georgia Institute of Technology Xie, Xing; Georgia Institute of Technology, Civil and Environmental Engineering; Georgia Institute of Technology |
| | |

Self-driven membrane filtration by core-shell polymer composites

Zeou Dou,¹ Ting Wang,¹ Wensi Chen,¹ Beichen Lin,¹ Hai Dong,² Wei Sun,² and Xing Xie^{1*}

¹School of Civil and Environmental Engineering, Georgia Institute of Technology, Atlanta, GA, USA.

²Tissue Mechanics Laboratory, The Wallace H. Coulter Department of Biomedical Engineering, Georgia Institute of Technology and Emory University, Atlanta, GA, USA.

*E-mail: xing.xie@ce.gatech.edu

Membrane filtration is an effective way of separation that usually requires an external driving force. Novel configurations simplifying the filtration process could offer extra versatility and enable separation in a broader context at different scales. This work presents a self-driven 3D filtration strategy based on core-shell polymer composites (CSPCs). The core is a hydrogel sphere that can spontaneously absorb ~50 times its own weight of water, while a polyamide film, as thin as ~7 nm, formed through interfacial polymerization serves as the separating shell. These flexible and easy-to-use CSPCs exhibit high-capacity and selective water absorption, which presents unique possibilities for applications such as concentrating biomedical and environmental samples for analyses and recovering valuable resources from waste streams.

Introduction

As a well-established separation process, membrane filtration plays a critical role in a variety of fields, including water purification, gas separation, bioprocessing, and chemical manufacturing, attributed to its favorable energy efficiency, compact footprint, and scalability.¹⁻³ In the era of increasingly pressing water and energy challenges, both highly permeable and selective membranes are made possible through (i) selective layer thickness control (down to sub-10 nm),^{4, 5} (ii) molecular-level morphology and pore-size design using alternative fabrication technique and novel polymeric materials,⁶⁻

¹¹ and (iii) novel sieving membranes (e.g., graphene and MoS₂).¹²⁻¹⁴ In traditional filtration processes, the filtrate is pushed through a filter under an external driving force, usually pressure. However, such a filter and the external driving force may not be available or favorable under certain circumstances where a simple and flexible separation solution is needed. For instance, when concentrating biomedical or environmental samples, if they are of very small volume and the target component to be concentrated is delicate, the conventional syringe filter could be damaging and cause the waste of the sample inside the syringe. In some other cases, in-situ liquid separation in a complex matrix is needed for on-site environmental monitoring or disease diagnosis, where the installation and operation of filtration devices is impossible.

Different from normal filtration processes where filtrate passes through either a flat or a curved cylinder-like filtration interface, in which case, the flow vector is either unidirectional (1D) or in the same plane (2D), a new concept of three-dimensional (3D) filtration using hydrogels was demonstrated recently for essentially spontaneous water filtration and enhanced mass transfer in an immersive setup, where the water flows into

the hydrogel absorbers from all directions.¹⁵⁻¹⁹ Hydrogels, a class of networks formed by crosslinking hydrophilic polymer chains, hold highly tunable and reversible properties under stimuli, attributed to which, they are widely used in various fields. In particular, when embedded with ionic groups, the hydrogel possesses a large capacity of water absorption (up to $\sim 1,000 \text{ g}\cdot\text{g dry gel}^{-1}$).²⁰ Attempts have been made to explore the potential of hydrogels for desalination, proving the water absorbing and solute rejecting ability of hydrogels for water separation. (Table 1). In one example, thermally responsive hydrogel discs of different crosslinking degrees were utilized to achieve brackish water (2 g/L NaCl) desalination through absorption and dewatering cycles. Only 23% salt content was removed at a moderate water absorption of $\sim 20 \text{ g}\cdot\text{g dry gel}^{-1}$.¹⁵ In another example, while a salt rejection of 65% was achieved, the water absorbency of the hydrogel absorber was very low at $\sim 3 \text{ g}\cdot\text{g dry gel}^{-1}$.¹⁶ Given the relatively small treating capacity, difficulties in continuous operation, and energy-intensive water recovery, hydrogel absorbers remain incompetent in large scale water purification applications. Nevertheless, the self-driven, flexible, and simple nature of hydrogel absorbers renders them rather promising in small scale applications such as

concentrating biological or environmental samples. Hydrogel spheres have been successfully utilized to fast concentrate microorganisms in water samples for reliable quantitative detection. Both bacteria and viruses could be effectively concentrated as the size of the water channels in the hydrogel spheres was only several nanometers.¹⁷

In addition to be applied for target quantification, hydrogel absorbers can also be utilized to concentrate valuable substances in aqueous solutions for more efficient transport and recovery. Hydrogel absorbers exhibiting a high water absorbency of $\sim 60 \text{ g}\cdot\text{g dry gel}^{-1}$ have been used to concentrate microalgae around 40 times to a high biomass concentration for biofuel extraction.¹⁹ In most cases, the rejection of solutes is achieved through size exclusion by controlling the pore size of the hydrogels which should be smaller than that of the target substances. The crosslinking ratio of the polymer chain network governs the pore size of the hydrogel. The higher the crosslinking ratio, the smaller the pore size, which means higher selectivity. However, the crosslinking ratio is inversely correlated to the absorbency of the hydrogel that determines the filtration capacity. Such trade-off makes the ideal hydrogel absorbers of both high selectivity and absorbency rather challenging.

In order to achieve self-driven 3D water filtration of both high selectivity and capacity for enhanced concentrating effect, we developed a core-shell polymer composites (CSPCs): A hydrogel sphere serves as the core driving water absorption, with a polyamide (PA) shell providing ion rejection (Fig. 1). Different from the molecular-level “core-shell” star block co-polymers utilized for the fabrication of anti-fouling nanofiltration membranes for traditional filtration,²¹ the innovative design of the macroscale core-shell configuration demonstrated here has never been reported. The core-shell configuration effectively tackles the trade-off between the selectivity and water absorbency and enables independent control over the two critical properties of such hydrogel absorbers. PA membrane as the active layer of thin film composite (TFC) membranes is widely used in nanofiltration and reverse osmosis.^{4, 7, 22} The combination of hydrogels and nanofiltration membranes has been reported in forward osmosis desalination process, however the unidirectional (1D) filtration interface hardly exploits the water absorbing ability of the hydrogels.²³ Given that, a 3D spherical core-shell configuration is advantageous. When the CSPC is immersed in an aqueous solution, water molecules diffuse into the network of the hydrogel, causing disentanglement and expanding of the hydrophilic network. The

absorbing pressure created by the volumetric swelling of the hydrogel keeps driving water intake until the equilibrium between the absorption and osmotic flow is reached. It is worthy to note that, instead of being driven by osmotic pressure like in FO processes, the water absorption in CSPCs is driven by the swelling pressure created by the expanding of the polymer network. The PA shell acts as a screen rejecting salt ions along the water absorption (Fig. 1). In this way, water filtration could happen spontaneously in these suspended 3D core-shell absorbers for extra versatility and control in separation processes using customized size and amount of the absorbers.

To the best of our knowledge, such 3D filtration based on dynamic core-shell polymer composites has never been reported before. Through interfacial polymerization (IP), an ultrathin PA shell was formed on the surface of the hydrogel core to obtain CSPC. With the innovative core-shell configuration enabling independent water absorbency and selectivity control over hydrogel composite absorbers, the CSPCs synthesized in this work achieved both high absorbency and selectivity presenting excellent separation performance in aqueous solutions (Table 1), which is especially useful in concentrating

valuable targets in complex aqueous matrixes for better detection, transport, and recovery.

Table 1 | Comparison of the existing hydrogel absorbers for 3D filtration

| Hydrogel composition | Shell | Morphology | Water absorbency | Selectivity control | Target | Rejection rate | Reference |
|--------------------------|-----------------|------------|-------------------------------|---------------------|-----------------|----------------|-----------|
| PSA-PNIPAM ^a | - | Disc | ~23 g·g dry gel ⁻¹ | Hydrogel | Na ⁺ | 23% | 15 |
| PSA-PHEMA ^b | - | Particle | ~3 g·g dry gel ⁻¹ | Hydrogel | Na ⁺ | 65% | 16 |
| P(AM-co-IA) ^c | - | Sphere | ~60 g·g dry gel ⁻¹ | Hydrogel | Bacteria | 98% | 17 |
| P(AM-co-IA) | - | Sphere | ~50 g·g dry gel ⁻¹ | Hydrogel | Bacteria | 87% | 18 |
| PAA ^d | - | Sphere | ~60 g·g dry gel ⁻¹ | Hydrogel | Microalgae | N/A | 19 |
| PSA-PAM ^e | PA ^f | Sphere | ~50 g·g dry gel ⁻¹ | Shell | Na ⁺ | 99% | This work |

^apoly(sodium acrylate)-poly(*N*-isopropylacrylamide), ^bpoly(sodium acrylate-co-2-hydroxyethyl methacrylate), ^cpoly(acrylamide-co-itaconic acid), ^dPolyacrylic acid, ^epoly(sodium acrylate)-polyacrylamide, ^fpolyamide

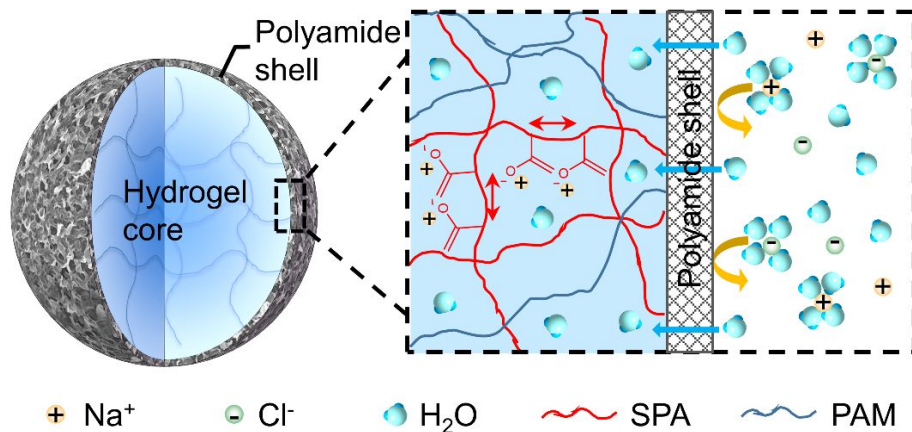


Fig. 1 | Schematic of the 3D water filtration based on the core-shell polymer composite (CSPC). The swelling of the hydrogel in an aqueous solution involves five steps: (i) the diffusion of water molecules into the crosslinked hydrophilic sodium polyacrylate (SPA) and polyacrylamide (PAM) polymer channels; (ii) the dissociation of the ionic species (Na^+) leaving the branches along the backbone long chains negatively charged; (iii) the relaxation and disentanglement of the polymer chains driven by the repelling force between likely charged branches; (iv) the expansion of the network creating negative pressure (swelling pressure) within the hydrogel, which continuously draws water inside the channels; and (v) the decrease of the swelling pressure along with the swelling until the equilibrium between the swelling and osmotic pressure is reached, at which point, the CSPC stops swelling. The PA shell rejects salt ions through size exclusion along the water absorption to achieve 3D water filtration.

Experimental section

Materials

Acrylic acid (AA), acrylamide (AM), tetrachloroethylene, toluene, ammonium persulfate (APS), N,N'-Methylenebisacrylamide (MBA), NaOH, ethanol (99.5%), m-phenylenediamine (MPD), trimesoyl chloride (TMC), and hexane were purchased from Sigma-Aldrich. Commercial maize bran (MB) without processing was purchased from local supermarket. Polydimethylsiloxane (PDMS) (Sylgard 184, Dow Chemical Co.).

Preparation of the CSPCs

To prepare the core of the CSPC, the aqueous monomer solution containing acrylic acid (AA) and Acrylamide (AM) was dropped into a mixed organic suspension phase comprised of tetrachloroethylene and toluene to form suspended individual monomer spheres. Then, the polymerization was carried out at 68°C for 30 min. As-prepared hydrogel spheres were dried in ethanol before use. To prepare the shell, the hydrogel spheres were immersed in MPD solutions of various concentrations, respectively, for 1 hour. The final diameter of the hydrogel spheres was ~10 mm. The obtained spheres were subsequently suspended in an organic suspension phase comprised of tetrachloroethylene and hexane containing difference concentrations of TMC for 2 mins, so that various PA shells were coated outside the hydrogel cores. The as-prepared CSPCs were suspended in 2M KCl before filtration experiments (see detailed information in Supplementary Text S2.1).

Water filtration experiments

The shrunken CSPCs (~3 mm) were transferred into 1 ml feed solution of different ion concentrations and species to initiate the swelling of CSPCs. The size change of the CSPCs was recorded by a digital microscope (Dini-Lite AM73915). The swelling was carried on for 45 mins.

The salt ion concentration of the stock solution and the residual solution was measured by atomic absorption spectroscopy (AAS) (PerkinElmer PinAAcle 900F). Sample volume was 0.5 ml (see detailed information in Supplementary Text S2.8).

Characterization

PA samples were separated from CSPCs and transferred onto different substrates for characterizations (see Supplementary Text S2.2). The thickness and roughness of the PA shells and flat membranes were measured by an atomic force microscope (AFM) (Veeco Dimension 3100). The morphology and surface features were observed by a scanning electron microscope (SEM) (Hitachi 8230) under 5 kV accelerating voltage and a transmission electron microscope (TEM) (Hitachi HT7700) under 120 kV accelerating voltage. The SEM samples were sputter coated with gold before characterization. In the swelling behavior study, wrinkle-fold evolution of the membrane was observed by an environmental SEM (ESEM) (Hitachi S-3700N) under 14 kV and 100 Pa. Elemental composition was measured by x-ray photoelectron spectrometer (XPS) (Thermo K-Alpha) equipped with an Ar ion sputter gun. Aluminum K-Alpha 1.486 KeV is used as the photoelectron source (see details in Supplementary Text S1.2). The cracking test of the PA shells was conducted under an optical microscope (Zeiss Axio observer 7). The Young's modulus of the Polydimethylsiloxane (PDMS) substrate for the wrinkling test was measured by a universal test machine (Testresources 100 series) (see details in Supplementary Text S2.6).

Results and discussion

The hydrogel spheres were synthesized with poly(sodium acrylate (PSA) and polyacrylamide (PAM) through suspension radical polymerization (Fig. S1). Figure 2A

shows the dried hydrogel spheres of a diameter of 1.9 ± 0.1 mm ($n > 10$). Hydrogel spheres of vastly different sizes (from less than 100 μm to several millimeters) can be fabricated through different procedures,²⁴ which makes CSPCs capable of water separation at different scales. The synthesis method and the size of the hydrogel spheres in this study was chosen for narrow size distribution and better characterization. The as-prepared hydrogel spheres were immersed in the aqueous *m*-phenylenediamine (MPD) solution (1 wt% in deionized water) to allow MPD molecules to enter the hydrogel network (Fig. 2B). While the swollen hydrogel sphere (10.8 ± 0.5 mm in diameter) (Fig. 2C) was suspended in an organic phase containing 0.03 wt% trimesoyl chloride (TMC), MPD molecules were released from the polymer channels to initiate IP on the surface of the hydrogel sphere, forming a PA shell (Figs. 2B & D). All the results shown in the following are based on the CSPCs fabricated from this MPD:TMC concentration combination (1 wt%:0.03 wt%), unless specified. Immersed in saline water (2M KCl), the CSPC gradually shrank to ~ 3 mm in diameter and became ready for swelling in different solutions to achieve water filtration (Fig. S2 and Fig. 2E).

Free-standing PA films separated from the hydrogel substrate were transferred onto different substrates for thorough characterization (Fig. S3). The PA shell prepared with 1% MPD showed a typical “ridge-and-valley” rough morphology with an apparent thickness of 64.3 ± 5.2 nm (Figs. 2F-G).⁶ This morphology can be easily tuned by changing the IP precursor concentration. When the MPD concentration was decreased to 0.1%, a smooth and ultrathin PA film, as thin as 7.4 ± 0.1 nm, was formed (Figs. 2H-I), indicating a controlled IP probably attributed to the unique diffusion of MPD molecules in the hydrogel network.⁴ The ultrathin PA shell offers possibility for ultrafast water absorption of the CSPCs.^{4, 5} The apparent thickness and roughness of the PA shell increased as the precursor concentration increased (Figs. S4-S5 and Table S1). As the MPD concentration increased, the PA shell of the final CSPC became increasingly wrinkled (Figs. 3A-D). The syntheses using different precursor concentrations resulted in PA shells with different morphology. The smooth PA shell made from 0.1% MPD had a roughness of only 0.4 ± 0.1 nm (Figs. 3E, I & M and Table S1). As the precursor concentration increased, small protruding nodules started to form on the shell surface (Fig. 3F). These nodules grew bigger and clustered together as the precursor

concentration further increased (Figs. 3G & H). The roughness increased accordingly (Table S1). When happening at relatively high reactant concentrations, the interfacial reaction generates heat faster than it can be dissipated. The Rayleigh-Bénard convection driven by the local heat accumulation,⁴ together with the limited diffusion of MPD molecules in the organic phase, causes the “local buoyancy and lateral inhibition” phenomenon at the interface.⁷ Further increased reactant concentration, meaning higher heat and diffusion instabilities, leads to the formation of small crumples on top of the increasingly curved up interface, which results in the “ridge-and-valley” rough PA shell structure covered by protruding nodules with sizes of 100 to 200 nm (Figs. 3J-L). As shown in TEM images, the nodules are mostly hollow with roughly 10-30 nm thick walls (Figs. 3N-P). The PA shell synthesized with high concentration MPD tends to have more nodule clusters of thick walls (~27 nm) (Figs. 3L & P).

The XPS results showed a similar surface atomic composition among the PA shells (Table S2). The relatively high oxygen concentration on the PA shell surface, especially the one fabricated with 2% MPD, is probably due to the oxidation of the precursor MPD

molecules during the prolonged absorption process before the interfacial polymerization.

The primary chemical shift is most likely attributed to the elements directly bonded to the carbon atom of interest, and the secondary shift (β -shift) is attributed to the strong electron withdrawing groups (amide and carboxylic acid) bonded to the carbon atom⁴. To quantify the bonding state of the atoms of interest, peak deconvolution was performed using CasaXPS software. The C1s peaks of the membranes were deconvoluted into five peaks at 284.8 eV (C-C, C=C, and C-H), 285.5 eV (β -shift for C-CONH, C-COO), 286.1 eV (C-N), 288.1 eV (N-C=O), and 289.0 eV (O-C=O). The narrow spectrum of O1s confirmed the amount of amide bond at 532.0 eV (N-C=O) and the unreacted acyl chloride group of TMC hydrolyzed to the carboxylic acid group at 533.2 eV (O-C=O). The amide bond at 400.0 eV (N-C=O) was found in the N1s spectrum with a small amount of unreacted amine at 401.5 eV (R-N⁺H₃)^{4,7} (Fig. S5 and Table S3).

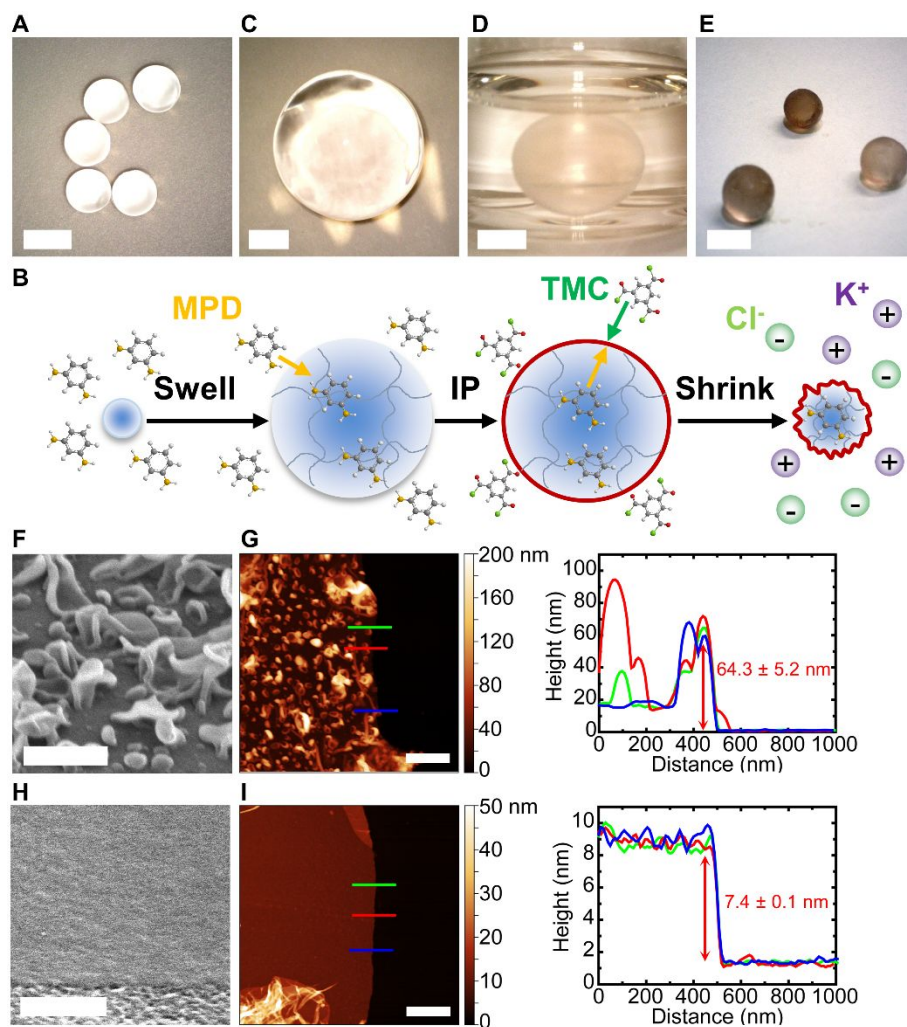


Fig. 2 | Fabrication and morphological characterization of the CSPCs. **A**, Photograph of dry hydrogel spheres. Scale bar, 2 mm. **B**, Schematics showing the CSPC fabrication. MPD, m-phenylenediamine; TMC, trimesoyl chloride. **C**, Photograph of a swollen hydrogel core containing MPD. Scale bar, 3 mm. **D**, Photograph of a CSPC suspended in the organic phase. Scale bar, 5 mm. **E**, Photograph of the CSPCs shrunk to different sizes. Scale bar, 5 mm. **F** and **H**, SEM images of the rough PA shell (1% MPD) and the smooth PA shell (0.1% MPD), respectively. Scale bars, 500 nm. **G** and **I**, AFM height images and corresponding height profiles of the rough PA shell (1% MPD) and the smooth PA shell (0.1% MPD) on top of a silicon wafer, respectively. Scale bars, 1 μm .

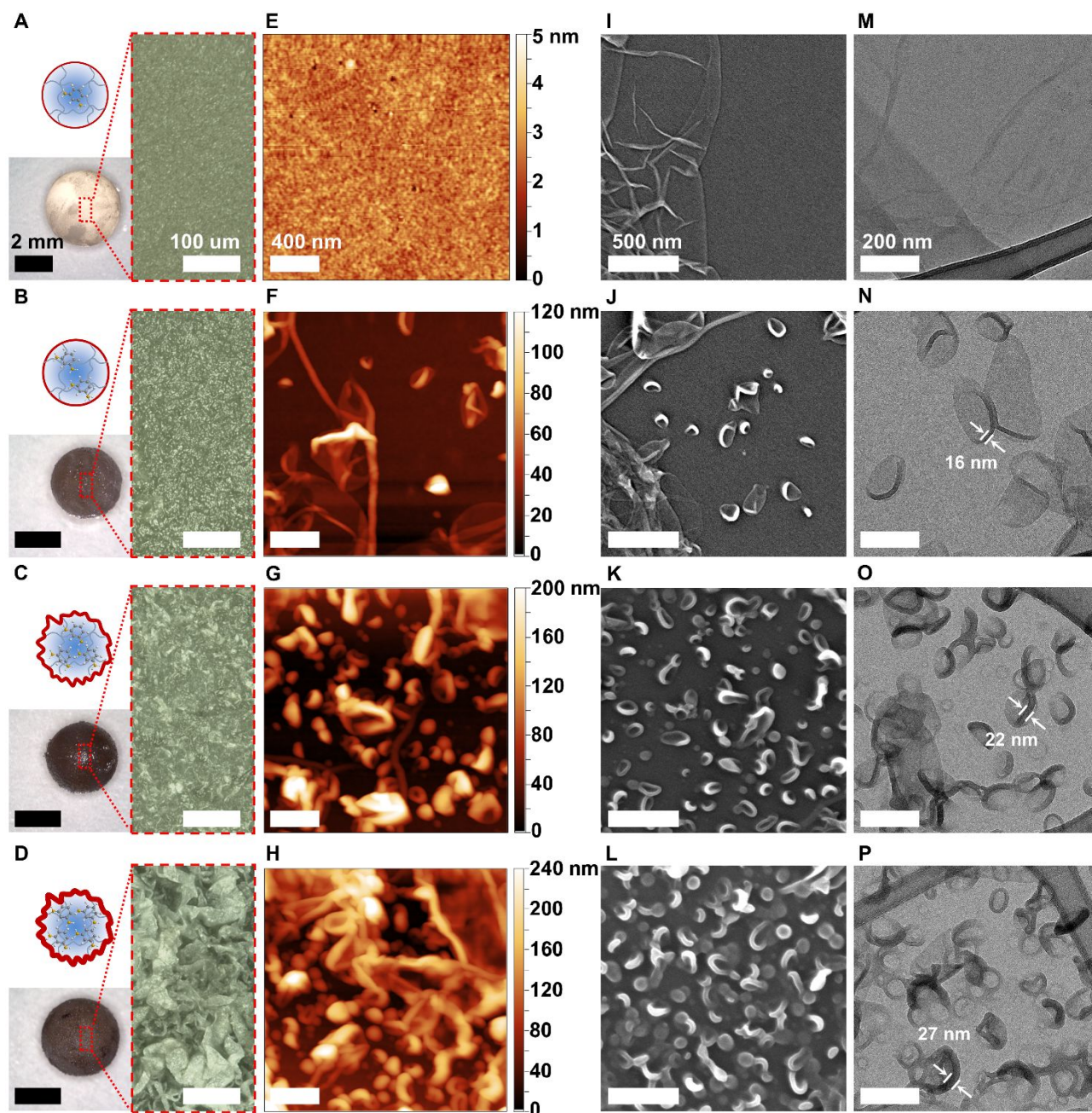


Fig. 3 | The CSPCs with different PA shells. A-D Schematics (left top), photographs (left bottom), and surface optical microscope images (right) of the final CSPCs: 0.1% MPD (**A**), 0.5% MPD (**B**), 1.0% MPD (**C**), and 2.0% MPD (**D**). **E-H**, AFM images of the PA shells made from 0.1% MPD (**E**), 0.5% MPD (**F**), 1.0% MPD (**G**), and 2.0% MPD (**H**). **I-L**, SEM images showing the surface structures on the PA shells made from 0.1%

MPD (**I**), 0.5% MPD (**J**), 1.0% MPD (**K**), and 2.0% MPD (**L**). **M-P**, TEM images of PA shells made from 0.1% MPD (**M**), 0.5% MPD (**N**), 1.0% MPD (**O**), and 2.0% MPD (**P**). The concentration ratio between MPD and TMC remained 20:1 for all the samples.

To withstand the swelling and shrinking of the CSPCs, mechanical endurance of the shells is crucial. Wrinkling-cracking measurements²⁵ were carried out on the flat-sheet hydrogel-based PA membranes (see experimental details in Supplementary Text S2.6, Figs. S6-S7). The membranes can be classified into two groups based on mechanical properties. Relatively smooth membranes exhibited much higher Young's modulus and fracture strength (e.g., 689.21 and 274.72 MPa, respectively, for 0.1% MPD membrane) than the rough ones did (e.g., 26.04 and 56.94 MPa, respectively, for 1% MPD membrane) (Fig. S7), indicating that the smooth PA membranes are more stiff and rigid while the rough ones are more elastic and flexible. These could be attributed to the dense isotropic structure of the smooth PA membranes²⁶ and the void-containing crumpled structure of the rough ones. Due to the difficulty in precise quantification of the thickness of the rough membrane samples, the reported mechanical properties are calculated from

average thickness from the AFM measurements. Thus, the results are only for comparison between different samples rather than absolute quantification.

The diameter of the CSPC increased from 3.2 ± 0.1 to 7.2 ± 0.1 mm in deionized water within 35 min (Fig. S8), corresponding to a water absorption of 52.8 ± 1.9 g·g dry gel⁻¹ (Fig. 4A). The coupled deformation and mass transport within the hydrogel core was simulated using a finite element method (mesh discretization) through COMSOL Multiphysics software based on Flory-Rehner free energy function²⁷ (see details in supplementary text S2.7). Along with the initial rapid swelling, the deformation transitioned from inhomogeneous to homogeneous within one second. The initial irregular surface deformation of the hydrogel was attributed to the finite triangular discretizing mesh elements mimicking the surface imperfection of the real hydrogel core. During homogeneous swelling, water diffusion within the hydrogel was driven by water concentration gradient along the sphere radius (Fig. 4B). The free energy of the swelling hydrogel is well depicted by the Flory-Rehner function²⁷ covering the entropy of the network expanding along with the mixing with the solvent molecules.²⁸ Given that, the

swelling of the hydrogel represents a process of hydrogel network entropy increasing caused by the decrease of the chemical energy embedded in the polymer chains. Therefore, the swelling behavior of hydrogels can be tailored according to three factors: (i) polymer density; (ii) mixing coefficient (hydrophilicity); and (iii) swelling stress (crosslink density), for preferable swelling rate and core-shell interaction to meet specific needs.

The relaxation of the rough PA shell (1% MPD) on the swelling CSPC (Figs. 4C-E) was recorded by ESEM (Figs. 4F-H). Before swelling, the PA shell on the shrunken CSPC wrinkled into hierarchical ridges to release the in-plane compression under the strain exerted by the spherical core (3D strain), as bending is more energetically efficient than compression²⁹ (Figs. 4F & I). During shell relaxation, the large amplitude ridges evolved into multi-wavelength wrinkles (Figs. 4G & J).^{29, 30} Further swelling of the CSPC resulted in the wrinkles of small amplitude but big wavelength (Figs. 4H & K). Such morphology evolution indicates a relatively loose attachment between the PA shell and the hydrogel core presenting a low risk of shell cracking under the 3D swelling strain.

Furthermore, no overlapping of the shell was observed on the shrunken CSPC implying trivial permeance hindrance.

Different from the rough shell (1% MPD) (Fig. 4F), the smooth shell (0.1% MPD) deformed predominantly into folds during the shrinking and retraced from arrayed deep folds to scattered shallow folds during the swelling (Fig. S9). This fold-dominant morphology with large contact area and tight adherence to the swelling substrate may make the smooth shell (0.1% MPD) susceptible to cracking. The notably different behavior of the smooth and rough shells under the 3D strain may be attributed to the different mechanical properties (Fig. S7). The more rigid and stiff the membrane is, the more likely the deformation of the membrane is focalized into folds.²⁹

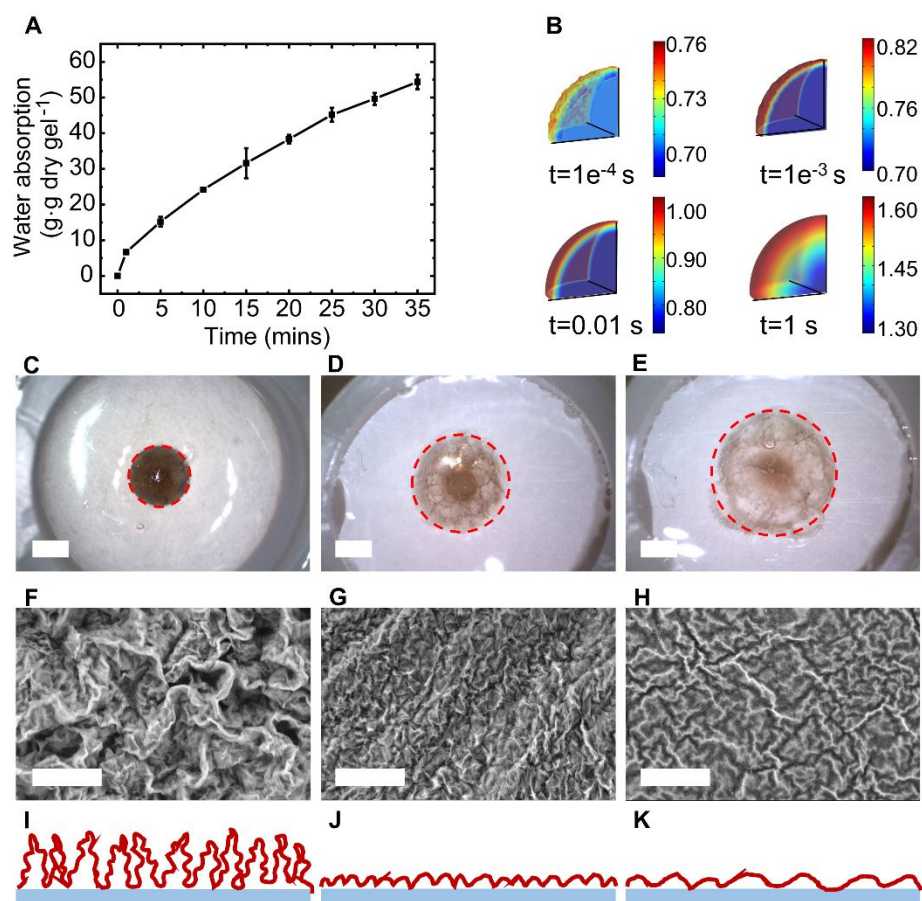


Fig. 4 | Swelling behaviour of the CSPCs. **A**, Water absorption of the CSPC plotted against swelling time. Error bars represent standard deviations from 3 independent experiments. **B**, The distribution of the deformation and water volume fraction within the swelling hydrogel sphere at different times by the finite element method simulation. The colour scale bar represents the water volume fraction (water volume/initial gel volume). **C-E**, Photographs of the swelling CSPCs at a diameter of ~3 mm (**C**), ~5 mm (**D**), and ~7 mm (**E**). The CSPC size was quantified based on the circle radius (red dashed circle). Scale bars, 2 mm. **F-H**, ESEM images showing the PA shells on the swelling CSPCs at a diameter of ~3 mm (**F**), ~5 mm (**G**), and ~7 mm (**H**). Scale bars, 30 μ m. **I-K**, Sketches

depicting the profile of the ridges (**I**), wrinkles of small wavelengths (**J**), and wrinkles of big wavelengths (**K**).

Methyl orange (MO) (molecular weight, $327.3 \text{ g}\cdot\text{mol}^{-1}$; volume, 0.86 nm^3)⁴ was used as a proof-of-concept indicator to demonstrate the selectivity of the CSPCs. The bare hydrogel sphere completely turned orange after swelling in the MO solution, while the hydrogel core of the CSPC remained colorless under identical conditions (Figs. 5A-B). To further quantify the selective permeability of the CSPCs, 3D filtration was also conducted in aqueous solutions with different ion concentrations and species. The CSPC swelled from 3.2 ± 0.1 to 6.7 ± 0.1 mm in $2 \text{ g}\cdot\text{l}^{-1}$ NaCl in 45 mins (Fig. S10). It is worth noting that, the residual MPD from the IP in the hydrogel network could negatively impact the water absorption ability of the hydrogel by forming hydrogel bonds with the polymer long chains restrain the relaxation and expansion of the network. Alternative shell synthesis methods involving no residual chemicals will be developed in the future work. The water absorption of the CSPC decreased as the salt concentration increased, as expected, due to the higher osmotic pressure of the feed solution (Fig. 5C). Although the salt rejection of the CSPC dropped from $99.8 \pm 0.4\%$ in $2 \text{ g}\cdot\text{l}^{-1}$ NaCl to $76.9 \pm 2.7\%$ in 4

$\text{g}\cdot\text{l}^{-1}$ NaCl, which was probably due to the stronger solute diffusion, no further decrease occurred in $6 \text{ g}\cdot\text{l}^{-1}$ NaCl (Fig. 5D). The CSPCs exhibited universally high salt rejection (>96%) in bivalent ion solutions (Fig. 5E). The similar water absorption ($40.6\text{-}42.8 \text{ g}\cdot\text{g dry gel}^{-1}$) in $2 \text{ g}\cdot\text{l}^{-1}$ NaCl achieved in the same amount of time (45 min) by the CSPCs with rough shells of increasing thickness (i.e., 0.5%, 1.0%, and 2.0% MPD) (Table S4) indicates that the water-absorbing hydrogel core is the rate limiting part of the CSPCs. By replacing the PAM with highly hydrophilic and biodegradable maize bran (MB), an even higher water absorption of $66.3 \text{ g}\cdot\text{g dry gel}^{-1}$ was achieved (Fig. S11). Moreover, it is worth noting that, although the ultrathin smooth PA shell (0.1% MPD) was particularly prone to defects during synthesis and swelling, it achieved a salt rejection close to 100% in $2 \text{ g}\cdot\text{l}^{-1}$ NaCl when remained intact. The 3D filtration tests in salt solutions show nanofiltration level selectivity of the CSPCs, which has never been realized by hydrogel absorbers, successfully demonstrating the concept of the core-shell hydrogel selective absorber. However, due to the intrinsic measurement error (5-10%) in current test procedures coming from the CSPC volume quantification and mild ion adsorption of the shell, the reported salt rejection data does not provide further indication on the structure and

rejection mechanism of the PA shells, which has been intensively studied in the literature.^{31, 32}

In addition, the CSPC (0.1% MPD) with intact shell, meaning good selectivity, exhibited higher water absorption, compared with the CSPC (0.1% MPD) with impaired shell (Fig. S12). When the shell is impaired, allowing external ions to enter the polymer network, the increased ion concentration will compress the electron double layer in the vicinity of the long chains, which constrains the ion dissociation. Consequently, the long chains become less charged and less likely to expand, leading to decreased swelling pressure, which is exhibited as the lower water absorption (Fig. S12). The experimental evidence further verifies our hypothesis on the mechanism of the water absorption by CSPCs introduced before (Fig. 1), which is different to the FO process.

The regeneration of the CSPCs was investigated, trying to recover the absorbed water and reuse the CSPCs. A simple evaporation test was carried out at 60 °C in an oven, which gave a water evaporation rate of 2.9 kg m⁻² h⁻¹. About 90% of absorbed water was evaporated within 2 hours. However, the PA shell became too crispy and fragile after

the drying process and shattered when immersed in the feed solution, which rendered the current CSPCs unfeasible to reuse. Enhancing the durability of the shells of the CSPCs will be one of the main topics for our follow-up research.

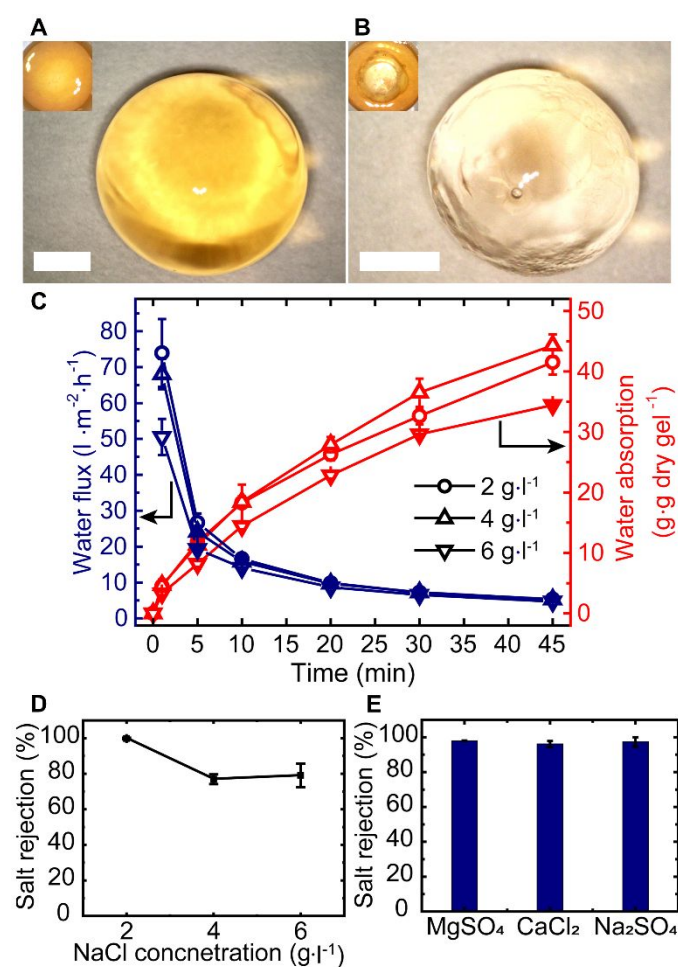


Fig. 5 | Demonstration of 3D water filtration by the CSPCs. A and B, Photographs of a bare hydrogel sphere (A) and a CSPC (B, with the shell peeled off) after swelling in the

methyl orange (MO) solution for 40 min. Scale bars, 3 mm. The insets show the bare hydrogel and the CSPC immersed in the MO solution, respectively. **C**, Water absorption of the CSPCs plotted against swelling time. Error bars represent standard deviations from 3 independent experiments. **D**, Salt rejection of the CSPCs swelling in NaCl solutions. **E**, Salt rejection of the CSPCs swelling in bivalent ion solutions with a cation molar concentration of 35 mM, which is equal to the Na⁺ molar concentration in 2 g·l⁻¹ NaCl. Error bars represent standard deviations from 3 independent experiments.

Perspectives

The spontaneous and highly selective (nanofiltration) water separation achieved by the flexible CSPCs can be appreciated in various fields in different scenarios. For example, in sample processing, CSPCs can easily absorb the excessive water while leaving substances of interest behind to achieve biomedical and environmental sample concentration, nanomaterial purification and harvesting, or nutrient (e.g., N, P) concentration and recovery in urine. After extracting pure water from unconventional water sources like salty water or wastewater, the swollen CSPCs can be transported and used as the water source for plants. In that case, water is released under the negative pressure generated by the plant roots. However, this self-driven filtration by CSPCs has its own limitations. Unlike traditional membrane filtration processes, the CSPCs are only

compatible with batch mode operations. The treating capacity of individual CSPC is restricted by its water absorbency. In addition, the reusability of the current CSPCs is limited by the insufficient mechanical strength and thermal stability of the PA shell, which compromises the cost-effectiveness of potential applications of the CSPCs. Moving forward, because the CSPCs eliminate the trade-off between the selectivity and absorbency, the structure and chemical composition of the hydrogel core could be conveniently modified for fast and reversible water absorption. For example, porous hydrogel core with thermo-responsiveness can be made for enhanced water uptake and recovery.^{15, 16} Besides heat, multi-stimuli responsive hydrogels can be made for “smart” control of water release for effective regeneration of the CSPCs.³³ On the shell side, cellulose, polybenzimidazole/polydopamine, chitosan/polyacrylic acid, and many other membranes of better endurance for recycling can be fabricated from various processes to replace the current PA membrane. Depending on the demand, shells of different levels of selectivity (e.g., nanofiltration, ultrafiltration, and microfiltration) can be coupled with the hydrogel core, presenting more possibilities for CSPCs. The prototype CSPC

demonstrated in this work offers a promising direction for the development of novel high-performance hydrogel absorbers.

Conclusions

Our results successfully demonstrated the concept of self-driven 3D filtration by CSPCs.

The novel core-shell structure eliminates the trade-off between the selectivity and absorbency of traditional hydrogel absorbers, which is critical for the realization of high ion rejection at a high water absorption. The CSPCs fabricated with the hydrogel core of PSA-PAM and the PA shell could absorb ~50 g water per g of the dry CSPCs. Applying these CSPCs for water filtration, we achieved >90% rejection for ions including Na⁺, Mg²⁺, and Ca²⁺. These easy-to-use, and flexible CSPCs possess great potentials in various fields.

Conflicts of interest

There are no conflicts to declare.

Acknowledgements

This work was performed in part at the Georgia Tech Institute for Electronics and Nanotechnology, a member of the National Nanotechnology Coordinated Infrastructure, which is supported by the National Science Foundation (Grant ECCS-1542174). Z.D. thanks Rebhadevi Monikandan for her suggestions on characterization methods and Martin Jacobson for helping make the mechanical test device. The authors would like to thank Guangxuan Zhu for his help on experimental set-ups and lab safety management.

Notes and references

1. H. B. Park, J. Kamcev, L. M. Robeson, M. Elimelech and B. D. Freeman, *Science*, 2017, **356**, eaab0530.
2. M. Elimelech and W. A. Phillip, *Science*, 2011, **333**, 712-717.
3. D. S. Sholl and R. P. Lively, *Nature News*, 2016, **532**, 435.
4. S. Karan, Z. Jiang and A. G. Livingston, *Science*, 2015, **348**, 1347-1351.
5. Z. Jiang, S. Karan and A. G. Livingston, *Advanced Materials*, 2018, **30**, 1705973.
6. J. R. Werber, C. O. Osuji and M. Elimelech, *Nature Reviews Materials*, 2016, **1**, 16018.
7. Z. Tan, S. Chen, X. Peng, L. Zhang and C. Gao, *Science*, 2018, **360**, 518-521.
8. Z. Wang, Z. Wang, S. Lin, H. Jin, S. Gao, Y. Zhu and J. Jin, *Nature Communications*, 2018, **9**, 2004.
9. J. K. Holt, H. G. Park, Y. Wang, M. Stadermann, A. B. Artyukhin, C. P. Grigoropoulos, A. Noy and O. Bakajin, *Science*, 2006, **312**, 1034-1037.
10. J. Chen, J. Zhang, X. Wu, X. Cui, W. Li, H. Zhang, J. Wang, X.-Z. Cao and P. Zhang, *Journal of Materials Chemistry A*, 2020, DOI: 10.1039/D0TA02150D.
11. D. Zhao, J. F. Kim, G. Ignacz, P. Pogany, Y. M. Lee and G. Szekely, *ACS Nano*, 2019, **13**, 125-133.
12. B. Mi, *Science*, 2019, **364**, 1033-1034.
13. G. R. Xu, J. M. Xu, H. C. Su, X. Y. Liu, L. Lu, H. L. Zhao, H. J. Feng and R. Das, *Desalination*, 2019, **451**, 18-34.

14. L. Ries, E. Petit, T. Michel, C. C. Diogo, C. Gervais, C. Salameh, M. Bechelany, S. Balme, P. Miele, N. Onofrio and D. Voiry, *Nature Materials*, 2019, **18**, 1112-1117.
15. W. Ali, B. Gebert, T. Hennecke, K. Graf, M. Ulbricht and J. S. Gutmann, *ACS Applied Materials & Interfaces*, 2015, **7**, 15696-15706.
16. C. Yu, Y. Wang, X. Lang and S. Fan, *Environmental Science & Technology*, 2016, **50**, 13024-13031.
17. X. Xie, J. Bahnemann, S. Wang, Y. Yang and M. R. Hoffmann, *Scientific Reports*, 2016, **6**, 20516.
18. X. Wu, X. Huang, Y. Zhu, J. Li and M. R. Hoffmann, *Separation and Purification Technology*, 2020, **239**, 116540.
19. C. Wei, Y. Huang, Q. Liao, Q. Fu, A. Xia and Y. Sun, *Bioresource Technology*, 2018, **249**, 713-719.
20. L. Yunkai, X. Tingwu, O. Zhiyun, L. Xiongcai, L. Honglu, H. Zhongyong and Y. Peiling, *Journal of Applied Polymer Science*, 2009, **113**, 3510-3519.
21. J. Diep, A. Tek, L. Thompson, J. Frommer, R. Wang, V. Piunova, J. Sly and Y. H. La, *Polymer*, 2016, **103**, 468-477.
22. M. R. Chowdhury, J. Steffes, B. D. Huey and J. R. McCutcheon, *Science*, 2018, **361**, 682-686.
23. A. Razmjou, Q. Liu, G. P. Simon and H. Wang, *Environmental Science & Technology*, 2013, **47**, 13160-13166.
24. E. M. Ahmed, *Journal of Advanced Research*, 2015, **6**, 105-121.
25. J. Y. Chung, J.-H. Lee, K. L. Beers and C. M. Stafford, *Nano Letters*, 2011, **11**, 3361-3365.
26. F. Foglia, S. Karan, M. Nania, Z. Jiang, A. E. Porter, R. Barker, A. G. Livingston and J. T. Cabral, *Advanced Functional Materials*, 2017, **27**, 1701738.
27. P. J. Flory and J. R. Jr., *The Journal of Chemical Physics*, 1943, **11**, 521-526.
28. W. Hong, X. Zhao, J. Zhou and Z. Suo, *Journal of the Mechanics and Physics of Solids*, 2008, **56**, 1779-1793.
29. P. Kim, M. Abkarian and H. A. Stone, *Nature Materials*, 2011, **10**, 952.

30. K. Efimenko, M. Rackaitis, E. Manias, A. Vaziri, L. Mahadevan and J. Genzer, *Nature Materials*, 2005, **4**, 293-297.
31. N. Y. Yip, A. Tiraferri, W. A. Phillip, J. D. Schiffman and M. Elimelech, *Environmental Science & Technology*, 2010, **44**, 3812-3818.
32. A. E. Childress and M. Elimelech, *Environmental Science & Technology*, 2000, **34**, 3710-3716.
33. F. G. Downs, D. J. Lunn, M. J. Booth, J. B. Sauer, W. J. Ramsay, R. G. Klemperer, C. J. Hawker and H. Bayley, *Nature Chemistry*, 2020, **12**, 363-371.